

Parametric-Resonance Production of QCD Axions

Pirzada 

CAS Key Laboratory of Theoretical Physics, Institute of Theoretical Physics,

Chinese Academy of Sciences, Beijing 100190, China and

School of Physical Sciences, University of Chinese Academy of Sciences, 19A Yuquan Road, Beijing 100049, China

Yu Gao *

State Key Laboratory of Particle Astrophysics, Institute of High Energy Physics,

Chinese Academy of Sciences, 19B Yuquan Road, Beijing 100049, China

Qiaoli Yang †

Physics Department, College of Physics and Optoelectronic Engineering, Jinan University, Guangzhou 510632, China

We demonstrate that dark matter axion production is enhanced through a natural and unavoidable mechanism: primordial temperature fluctuations periodically modulate the axion mass during the QCD phase transition, thereby triggering parametric resonance in axion field evolution. This interplay between parametric resonance and the misalignment mechanism shifts the predicted axion mass window for the observed dark matter abundance to $10^{-4} - 10^{-3}$ eV, displacing the canonical axion mass window to previously unexplored higher ranges.

Introduction. Observations from galaxy dynamics, precision cosmic microwave background (CMB) measurements, and large-scale structures establish that dark matter constitutes 27% of the cosmic energy budget [1, 2]. However, the fundamental nature of dark matter remains elusive. Among proposed candidates, the QCD axion is particularly well-motivated: it was introduced to resolve the strong CP problem by breaking a global $U(1)$ Peccei-Quinn symmetry that dynamically relaxes the QCD θ -angle [3–5], with current benchmark models including the KSVZ [6, 7] and DFSZ [8, 9] axions. QCD axion dark matter is predominantly produced via the misalignment mechanism [10–12]. This mechanism generally predicts a QCD axion mass around 10^{-5} eV. If the axion field existed prior to inflation, its quantum fluctuations would imprint isocurvature perturbations in the CMB, leading to stringent observational constraints [13–18].

In this Letter, we present a novel and complementary mechanism for generating QCD axion dark matter in the early universe. Primordial density fluctuations from inflation induce periodic temperature variations during the QCD phase transition. These temperature fluctuations modulate the axion mass, triggering parametric resonance—a nonlinear phenomenon in which energy is exponentially transferred when the modulation frequency matches the harmonics of the field’s oscillation frequency. Characterized by instability bands in Mathieu-type dynamics [19–21], this process amplifies the axion production by orders of magnitude, which survive cosmic expansion as a nonrelativistic population, creating a relic density that supplements the homogeneous misalignment mechanism. A parametric-resonance mechanism driven by scalar perturbations was proposed in [21]. We perform the first comprehensive study of this mechanism in a realistic cosmological setting and quantify its impact on the axion relic abundance. This mechanism exhibits

three key features: *First*, it is sourced by temperature fluctuations rather than an initial condition. *Second*, the mechanism evades the isocurvature constraints [22]. *Third*, it is naturally occurring as $m_a(T)$ fluctuates near the QCD phase transition epoch. Unlike previous studies of resonant axion excitation that redistribute an existing axion population [23], we demonstrate a parametrically driven resonance sourced by primordial temperature fluctuations, populating axion modes independently of the initial field amplitude. Due to this mechanism, the predicted dark matter QCD axion mass ($m_a \sim 10^{-5}$ eV) is shifted to a heavier range. This could explain the current null experimental results and motivate future experiments to target higher frequency ranges [24–28].

Field dynamics. The axion field $\phi(\vec{x}, t)$ obeys the Klein–Gordon equation:

$$D^\mu \partial_\mu \phi(\vec{x}, t) - m^2(T) \phi(\vec{x}, t) = 0 , \quad (1)$$

where D^μ is the covariant derivative and $m(T)$ is the temperature-dependent axion mass that evolves with the cosmological temperature $T(t)$. To incorporate leading-order scalar perturbations, we work in the conformal Newtonian gauge and retain terms linear in the metric potentials Φ and Ψ . The resulting equation of motion becomes

$$\ddot{\phi} + 3H\dot{\phi} - \frac{1}{a^2} \nabla^2 \phi + m^2(T) \phi + f(\vec{x}, t, \phi) = 0 , \quad (2)$$

where the function $f(\vec{x}, t, \phi)$ encodes scalar perturbations and includes: (i) renormalization of the kinetic operator, (ii) a modified friction term, (iii) gradient effects from the perturbed spatial metric, and (iv) modulation of the effective mass (see supplementary material for derivations).

Explicitly:

$$f(\vec{x}, t, \phi) = -2\Psi \ddot{\phi} - (\dot{\Psi} - 3\dot{\Phi} + 6H\Psi) \dot{\phi} + \frac{2\Phi}{a^2} \nabla^2 \phi - \frac{1}{a^2} \partial_j (\Phi + \Psi) \partial_j \phi + \frac{dm^2}{dT} \delta T \phi. \quad (3)$$

The resonance parameters are time-dependent, causing the instability band to sweep through momentum space. The system is driven by a stochastic primordial potential. To capture the full dynamics without assuming a small q or adiabatic band-crossing, we solve the mode equation numerically and perform an ensemble average over realizations of the primordial perturbation.

Equation 2 exemplifies the canonical setup for parametric resonance: a damped oscillator with a time-dependent frequency and periodic mass modulation sourced by scalar metric perturbations. During radiation domination, the scale factor evolves as $a(t) = (t/t_1)^{1/2}$, and the comoving wavenumber scales as $k^2/a^2(t) = k^2 t_1/t$, where t_1 denotes the time when oscillations begin. The unperturbed, homogeneous Φ equation is

$$\ddot{\phi}(\vec{k}, t) + \frac{3}{2t} \dot{\phi}(\vec{k}, t) + \omega_k^2(t) \phi(\vec{k}, t) = 0 \quad (4)$$

with $\omega_k^2(t) \equiv k^2 t_1/t + m^2(t)$. Resonance effects arise from the terms in $f(\vec{x}, t, \phi)$. Substituting the sub-horizon radiation-era solution for $\Phi(\vec{k}, t)$ and the temperature perturbation $\delta T/T$ [29], and retaining leading resonant harmonics, yields the k -space equation:

$$\begin{aligned} & \left[1 - \frac{9\Phi_p(\vec{k})}{2k^2 t t_1} \cos \Theta_k(t) \right] \ddot{\phi}(\vec{k}, t) + \\ & \left[\frac{3}{2t} + \frac{9\Phi_p(\vec{k})}{\sqrt{3} k t^2} \sqrt{\frac{t}{t_1}} \sin \Theta_k(t) - \frac{27\Phi_p(\vec{k})}{4k^2 t^2 t_1} \cos \Theta_k(t) \right] \dot{\phi}(\vec{k}, t) \\ & + \left[k^2 \frac{t_1}{t} + m^2(t) + \left(\frac{9\Phi_p(\vec{k})}{2t^2} - \frac{3\Phi_p(\vec{k})}{2} \frac{dm^2(t)}{dT} T(t) \right) \right. \\ & \left. \times \cos \Theta_k(t) \right] \phi(\vec{k}, t) = 0, \end{aligned} \quad (5)$$

Here, $a(t_1) = 1$ is adopted for simplicity. The phase $\Theta_k(t) \equiv 2k\sqrt{t_1 t/3}$ arises from acoustic oscillations of the radiation fluid potential $\Phi \propto \cos(k\eta/\sqrt{3})$, where conformal time η is converted to cosmic time via $\eta(t) = \int^t dt'/a(t') = 2\sqrt{t t_1}$. The time t_1 marks the onset of axion oscillations and is implicitly defined by

$$t_1 \simeq (t_2^{2n}/m^2)^{\frac{1}{2n+2}}, \quad (6)$$

with the QCD transition time $t_2 \sim 10^{-5}$ s at a temperature $T \sim 100$ MeV [30]. For mass-temperature we adopt the powerlaw relation $m_a(T) \propto T^{-n}$ and take $n = 3$ as given by lattice results [31–35].

Equation 5 reveals three distinct modulation channels: (i) the $\dot{\phi}$ term renormalizes effective inertia, (ii) the $\dot{\phi}$ term modulates friction, and (iii) the remaining terms involve mass modulation via $(dm^2/dT)T$, sourced by δT . As $m(t)$ increases during the QCD phase transition, this mass modulation dominates energy injection. While $m(t)$ introduces nontrivial time dependence, useful approximations emerge by isolating dominant terms and recasting the equation into Mathieu-type form.

Parametric resonance is most efficient when the periodic drive is near twice the instantaneous frequency (e.g., the $l = 2$ band), or more generally near integer harmonics:

$$\omega_{\text{drive}}(t) \simeq l \omega_k(t), \quad l = 1, 2, 3, \dots \quad (7)$$

The driving frequency is determined by the phase in Eq. (5). The dominant ($l = 2$) resonance condition $\omega_{\text{drive}} \simeq 2\omega_k$ implies a short-lived resonance event for each k -mode:

$$t_R = \begin{cases} t_2 \left(\frac{k}{k_2} \right)^{\frac{2}{2n+1}} & \text{for } k < k_2, \\ t_2 \left(\frac{k}{k_2} \right)^2 & \text{for } k > k_2, \end{cases} \quad (8)$$

depending on whether the resonance occurs during the growth phase $t_1 \leq t \leq t_2$ or after mass growth saturates. Here, k_2 denotes a reference scale: $k_2 \equiv m\sqrt{3t_2/t_1}$.

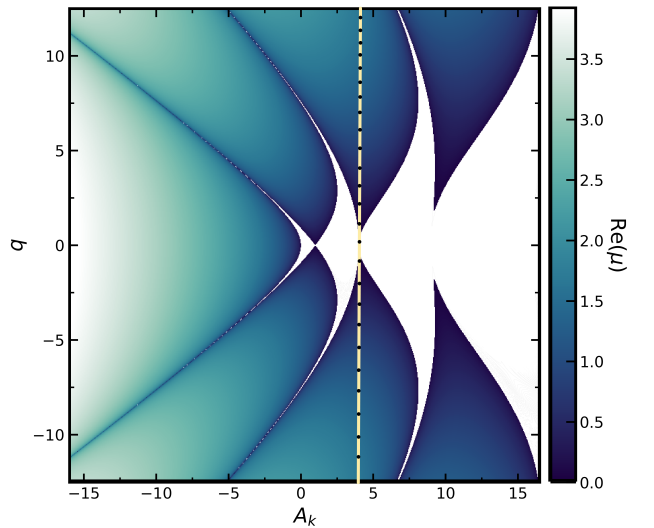


FIG. 1. Mathieu instability chart showing the largest Floquet exponent $\text{Re}(\mu)$ in the (A_k, q) plane. Colored regions indicate parametric resonance ($\text{Re}(\mu) > 0$); the black contour outlines the instability boundary, and the vertical line marks the $l = 2$ resonance center at $A_k = 4$.

During the brief interval around $t \simeq t_R(k)$, the coefficients in Eq. (5) vary slowly compared to the oscillatory phase. Neglecting Hubble friction and cosmic expansion over this narrow window, the mode equation reduces to

a Mathieu-type form by introducing the rescaled time variable:

$$z \equiv \frac{k}{\sqrt{3}} \eta(t) = 2k \sqrt{\frac{tt_1}{3}}, \quad (9)$$

which transforms oscillatory terms into sinusoidal dependence on z . After a field redefinition to remove the leading first-derivative term, the mode equation becomes canonical (see supplementary material):

$$\partial_z^2 \phi_k + (A_k - 2q \cos 2z) \phi_k = 0, \quad (10)$$

with Mathieu parameters:

$$A_k = 3 + \frac{3m^2(t)}{k^2}, \quad q = \frac{dm^2(t)}{dT} \frac{9\Phi_p(\vec{k})T(t)}{4k^2}. \quad (11)$$

Instability bands occur when $A_k \simeq l^2$ for integer l . The dominant $l = 2$ band corresponds to $A_k \simeq 4$, and for small parameter q , the band width scales as $\Delta A_k \sim q^2$. The growth rate $\mu(t) \equiv d \ln |\phi_k|/dt$ illustrates the resonance behavior, as shown in Fig. 1.

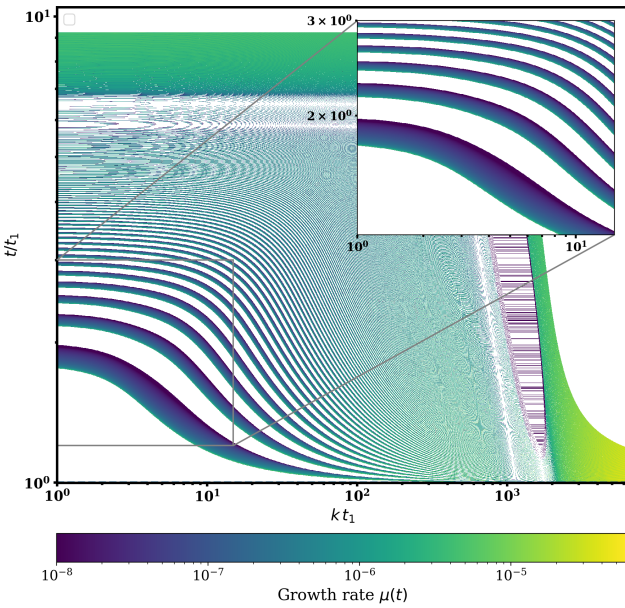


FIG. 2. Resonance band-map computed from the full equation of motion. The instantaneous growth rate $\mu(\tau, \kappa) \equiv t_1^{-1} d \ln |\phi(\tau; \kappa)|/d\tau$ is derived from numerical solutions of Eq. (5). Stable regions between bands are left blank. Band structures widen and become more visible in the weak-driving regime (lower-left). Broken patterns near 2×10^3 reflect numerical precision limits.

Full dynamics is richer than the qualitative discussion with the narrow-resonance Mathieu analysis above. Simulation reveals recurring short-time resonant behavior when Eq. (5) is solved numerically and the field growth rate is plotted over the dimensionless (κ, τ) plane (Fig. 2), where $\kappa \equiv kt_1$ and $\tau \equiv t/t_1$. The resulting instability bands pinpoint epochs where periodic metric-sourcing

terms efficiently produce axions. A single k -mode typically encounters multiple resonance bands during the phase transition, with band locations drifting over time. This drift arises because both the effective frequency $\omega_k^2(\tau) = k^2/a^2 + m^2(\tau)$ and the driving amplitude evolve across the transition near $t \simeq t_2$. For larger k , parametric drive dominates growth. Resonant bands progressively narrow and densely cluster as k increases, with growing structural complexity.

Relic density of the resonance-enhanced growth is calculated through numerical integration of Eq. 5, which we then compare to the homogeneous case. First, a baseline solution $\phi_b(t, k)$ for misalignment is computed by solving the homogeneous Eq. 4 with initial conditions $\phi_b(t_1, k) = \theta_0 f_a$, and $\dot{\phi}_b(t_1, k) = 0$, where θ_0 denotes the initial misalignment angle. Second, we isolate the resonance-generated component as $\phi_1(t, k; \Phi_p) \equiv \phi_f(t, k; \Phi_p) - \phi_b(t, k)$, ensuring both ϕ_1 and $\dot{\phi}_1$ vanish at t_1 . The system is driven by primordial fluctuations with a nearly scale-invariant power spectrum [22]:

$$\mathcal{P}_\Phi(k) \equiv \frac{k^3}{2\pi^2} \langle |\Phi(\mathbf{k})|^2 \rangle. \quad (12)$$

We restrict to the linear regime and adopt a k -independent amplitude [23] $\langle |\Phi_p(k)|^2 \rangle = \mathcal{P}_\Phi(k) \simeq A$, with $A \simeq \mathcal{O}(10^{-9})$ [36].

Since Eq. 5 is linear in Φ_p , the resonance-generated field satisfies $\phi_1(t, k; \Phi_p) \propto \Phi_p$, leading to axion energy densities scaling quadratically with Φ_p . Our numerical procedure solves the equations for fixed realizations of Φ_p and averages over Gaussian-distributed Φ_p with $\langle \Phi_p \rangle = 0$ and $\text{Var}(\Phi_p) = A$. The energy density for each mode is

$$E_1(t, k; \Phi_p) = \frac{1}{2} \dot{\phi}_1^2(t, k; \Phi_p) + \frac{1}{2} \omega_k^2(t) \phi_1^2(t, k; \Phi_p), \quad (13)$$

and the ensemble-averaged spectral energy density per logarithmic interval is

$$\frac{d\rho_1}{d \ln k}(t, k) \equiv \langle E_1(t, k; \Phi_p) \rangle_{\Phi_p}. \quad (14)$$

The total energy density is obtained by integrating over resonant modes $k \in [t_1^{-1}, k_2]$, as defined in Eq. 8, to set a conservative upper bound. As shown in Fig. 2, higher- k modes resonate earlier and experience greater redshift by t_2 . In simulations, the majority of resonance-enhanced modes become nonrelativistic by the end of the QCD phase transition.

Equation 14 still retains spatial gradients that redshift differently from nonrelativistic matter. This component is negligible if boosted modes are nonrelativistic. To quantify today's relic density, we define a “diluted ratio” $\Gamma \equiv \tilde{\rho}_1/\rho_0$, where tilde excludes spatial gradient terms in ρ_1 , and $\rho_1/\rho_0 \rightarrow \Gamma$ at low redshift. The present-day dark matter fraction is then

$$\Omega = (1 + \Gamma) \frac{\rho_0(t_*; m)}{\rho_{c,0}} \left(\frac{a_*}{a_0} \right)^3, \quad (15)$$

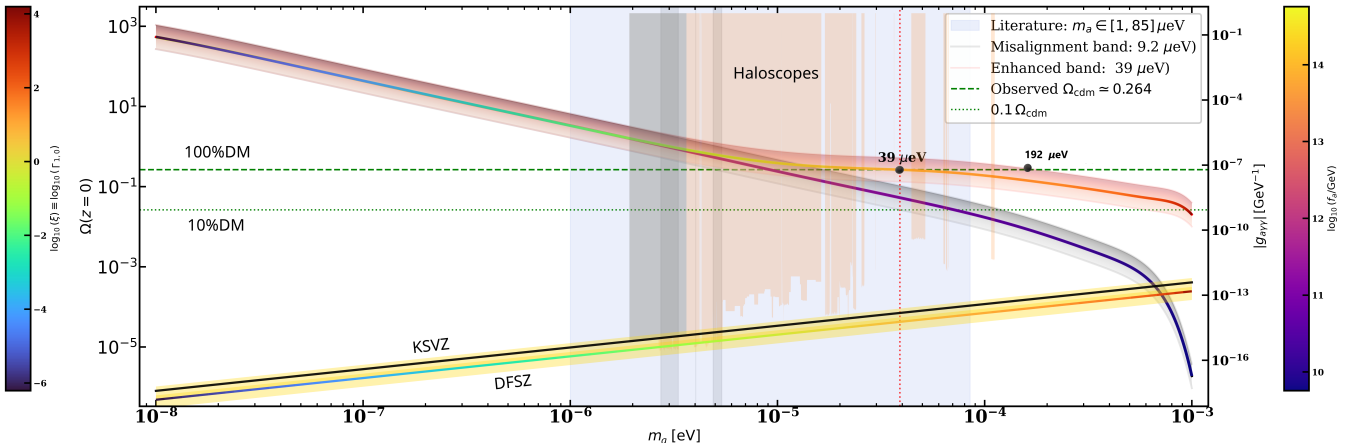


FIG. 3. Parametric Resonance’s impact on the QCD axion relic abundance. Homogeneous misalignment (gray) and resonance-enhanced (red) predictions are shown as bands, with widths reflecting the initial misalignment angle $\theta_0 \in [1, 2]$. A benchmark case with $\theta_0 = 1.3$ is highlighted via solid curves through the band centers. Resonance-enhanced scenarios account for 100% dark matter at axion masses 39 (192) μeV for $\theta_0 = 1.3$ (2.0). For comparison, literature predictions and existing haloscope constraints [37] are overlaid. The lower band (yellow) illustrates the mass-coupling relation across QCD axion models.

with $\rho_{c,0}$ as today’s critical density and ρ_0 the misalignment energy density [10, 11, 38]. Here, t_* and a_* denote the time and scale factor at the end of mass modulation.

Results & Discussion. We compute the parametric resonant equations for an axion mass range $m \in [10^{-8}, 10^{-3}]$ eV. Imposing an upper limit $m \leq 10^{-3}$ eV ensures the parameter q remains small, avoiding excessively large perturbations. Predictions for present-day relic density are illustrated in Fig. 3. We assume an $\mathcal{O}(1)$ initial misalignment angle $\theta_0 \in [1, 2]$ to be consistent with unexplored regions in the classical window. While the choice of θ_0 shifts overall predictions for both scenarios, the ratio between resonance-enhanced and homogeneous misalignment abundances remains θ_0 -independent.

Parametric resonance redefines the QCD axion dark matter target by significantly enhancing the relic abundance for masses above 10^{-5} eV. If misalignment alone explains the observed dark matter density, parametric resonance raises the preferred axion mass from $\sim 10 \mu\text{eV}$ to $39 \mu\text{eV}$ and $192 \mu\text{eV}$ for $\theta_0 = 1.3$ and 2, respectively—masses exceeding the sensitivity of current haloscope experiments. These preferred values for 100% dark matter remain subject to cosmological uncertainties in plasma modeling and primordial perturbations.

For low masses ($m \ll 10 \mu\text{eV}$), a smaller θ_0 is typically assumed. From Eq. 11, the parameter $q \propto dm^2/dT$, so a smaller axion mass quadratically reduces the pumping efficiency, suppressing resonance effectiveness in this regime. If misalignment accounts for only a fraction of the relic abundance (as between the 10% and 100% DM lines in Fig. 3), parametric resonance provides sufficient density boosts at $10^{-4} - 10^{-5}$ eV to meet observational requirements.

To summarize, we demonstrate in this Letter that

mass parametric resonance seeded by primordial perturbations provides a natural and robust mechanism for cosmic QCD axion production as dark matter. This process predicts an upward shift in the axion mass window, overcoming underproduction inherent to homogeneous misalignment scenarios in genuine QCD axion models. We present the first comprehensive treatment of mass-oscillation-driven field evolution, showing that parametric resonance band maps predict recurring growth episodes where energy is transferred from the plasma environment into axion populations. Analysis via Mathieu-type simplification during resonance windows reveals reoccurring strong energy transfer at larger axion masses and lower k . Since environmental modulation is intrinsic to plasma physics, this advocates parametric resonance as an inevitable, inflation-seeded phenomenon for QCD axions and a broadly applicable mechanism for light bosonic dark matter production.

Acknowledgments. The authors thank Nadir Ijaz for assistance with numerical implementation. This work was supported in part by the National Natural Science Foundation of China (Grant No. 12447105).

* gaoyu@ihep.ac.cn

† qiaoliyang@jnu.edu.cn

- [1] M. Persic, P. Salucci, and F. Stel, The Universal rotation curve of spiral galaxies: 1. The Dark matter connection, *Mon. Not. Roy. Astron. Soc.* **281**, 27 (1996), arXiv:astro-ph/9506004.
- [2] N. Aghanim *et al.* (Planck), Planck 2018 results. VI. Cosmological parameters, *Astron. Astrophys.* **641**, A6 (2020), [Erratum: Astron. Astrophys. 652, C4 (2021)], arXiv:1807.06209 [astro-ph.CO].

[3] R. D. Peccei and H. R. Quinn, Cp conservation in the presence of pseudoparticles, *Phys. Rev. Lett.* **38**, 1440 (1977).

[4] R. D. Peccei and H. R. Quinn, Constraints imposed by cp conservation in the presence of instantons, *Phys. Rev. D* **16**, 1791 (1977).

[5] S. Weinberg, A new light boson?, *Phys. Rev. Lett.* **40**, 223 (1978).

[6] J. E. Kim, Weak-interaction singlet and strong cp invariance, *Phys. Rev. Lett.* **43**, 103 (1979).

[7] M. A. Shifman, A. I. Vainshtein, and V. I. Zakharov, Can confinement ensure natural cp invariance of strong interactions?, *Nucl. Phys. B* **166**, 493 (1980).

[8] M. Dine, W. Fischler, and M. Srednicki, A simple solution to the strong cp problem with a harmless axion, *Phys. Lett. B* **104**, 199 (1981).

[9] A. R. Zhitnitsky, On possible suppression of the axion hadron interactions, *Sov. J. Nucl. Phys.* **31**, 260 (1980).

[10] J. Preskill, M. B. Wise, and F. Wilczek, Cosmology of the invisible axion, *Phys. Lett. B* **120**, 127 (1983).

[11] L. F. Abbott and P. Sikivie, A cosmological bound on the invisible axion, *Phys. Lett. B* **120**, 133 (1983).

[12] M. Dine and W. Fischler, The not-so-harmless axion, *Phys. Lett. B* **120**, 137 (1983).

[13] M. P. Hertzberg, M. Tegmark, and F. Wilczek, Axion cosmology and the energy scale of inflation, *Phys. Rev. D* **78**, 083507 (2008).

[14] J. Hamann, S. Hannestad, G. G. Raffelt, *et al.*, Cosmological constraints on neutrino and axion hot dark matter, *JCAP* **06**, 022.

[15] O. Wantz and E. P. S. Shellard, Axion cosmology revisited, *Phys. Rev. D* **82**, 123508 (2010).

[16] M. Beltran, J. Garcia-Bellido, and J. Lesgourgues, Bounds on hot dark matter particles with entropic degrees of freedom, *Phys. Rev. D* **75**, 103507 (2007).

[17] N. Ijaz, M. Mehmood, and M. U. Rehman, The stochastic gravitational-wave background from primordial black holes and observable proton decay in R-symmetric SU(5) Inflation, *Eur. Phys. J. C* **85**, 1394 (2025), arXiv:2308.14908 [astro-ph.CO].

[18] N. Ijaz and M. U. Rehman, Exploring primordial black holes and gravitational waves with R-symmetric GUT Higgs inflation, *Phys. Lett. B* **861**, 139229 (2025), arXiv:2402.13924 [astro-ph.CO].

[19] N. W. McLachlan, Theory and application of mathieu functions, *The Mathematical Gazette* **52** (1968).

[20] L. Kofman, A. D. Linde, and A. A. Starobinsky, Towards the theory of reheating after inflation, *Phys. Rev. D* **56**, 3258 (1997).

[21] R. Zheng, P. Wei, and Q. Yang, Generation of axions and axion-like particles through mass parametric resonance induced by scalar perturbations in the early universe, *Chin. Phys. B* **49**, 125108 (2025), arXiv:2507.13127 [hep-ph].

[22] Y. Akrami *et al.* (Planck), Planck 2018 results: X. constraints on inflation, *Astron. Astrophys.* **641**, A10 (2020).

[23] P. Sikivie and W. Xue, Resonant excitation of the axion field during the qcd phase transition, *Phys. Rev. D* **105**, 043533 (2022).

[24] P. Pralavorio (MADMAX), The axion dark matter experiment MADMAX, *PoS ICHEP2024*, 751 (2025), arXiv:2409.20169 [hep-ex].

[25] Wei *et al.*, New constraints on dark photon dark matter with a millimeter-wave dielectric haloscope, *Phys. Rev. Lett.* , (2026).

[26] L. H. Nguyen, D. Horns, and A. Lobanov, Permanently magnetized axion-photon conversion surface for direct dark matter searches with BRASS-p, *JINST* **20** (12), P12026, arXiv:2509.20583 [physics.ins-det].

[27] S. Knirck *et al.* (BREAD), First Results from a Broadband Search for Dark Photon Dark Matter in the 44 to 52 μ eV Range with a Coaxial Dish Antenna, *Phys. Rev. Lett.* **132**, 131004 (2024), arXiv:2310.13891 [hep-ex].

[28] B. Ahmad, Y.-A. Liu, and N. Houston, Resonant enhancement of axion dark matter decay (2025), arXiv:2507.18508 [hep-ph].

[29] S. Dodelson, *Modern Cosmology* (Academic Press, Amsterdam, 2003) p. 196.

[30] L. Husdal, On effective degrees of freedom in the early universe, *Galaxies* **4**, 78 (2016).

[31] S. Borsányi, Z. Fodor, J. Guenther, K.-H. Kampert, S. D. Katz, T. Kawanai, T. G. Kovács, *et al.*, Calculation of the axion mass based on high-temperature lattice quantum chromodynamics, *Nature* **539**, 69 (2016), arXiv:1606.07494 [hep-lat].

[32] P. Petreczky, H.-P. Schädler, and S. Sharma, The topological susceptibility in finite temperature qcd and axion cosmology, *Physics Letters B* **762**, 498 (2016), arXiv:1606.03145 [hep-lat].

[33] A. Athenodorou, C. Bonanno, C. Bonati, G. Clemente, F. D'Angelo, M. D'Elia, L. Maio, G. Martinelli, F. Sanfilippo, and A. Todaro, Topological susceptibility of $n_f = 2 + 1$ qcd from staggered fermions spectral projectors at high temperatures, *Journal of High Energy Physics* **2022**, 197 (2022), arXiv:2208.08921 [hep-lat].

[34] Y.-C. Chen, T.-W. Chiu, and T.-H. Hsieh, Topological susceptibility in finite temperature qcd with physical $(u/d, s, c)$ domain-wall quarks, *Physical Review D* **106**, 074501 (2022), arXiv:2204.01556 [hep-lat].

[35] A. Y. Kotov, M. P. Lombardo, and A. Trunin, Topological observables and θ dependence in high temperature qcd from lattice simulations, *Journal of High Energy Physics* **2025**, 045 (2025).

[36] S. Naess *et al.*, The atacama cosmology telescope: Dr6 maps, *JCAP* , 061arXiv:2503.14451 [astro-ph.CO].

[37] C. O'Hare, cajohare/axionlimits: Axionlimits, <https://cajohare.github.io/AxionLimits/> (2020).

[38] P. Sikivie and Q. Yang, Bose-einstein condensation of dark matter axions, *Phys. Rev. Lett.* **103**, 111301 (2009).

[39] R. N. Bracewell, The fourier transform and its applications (1966).

[40] V. Mukhanov, *Physical foundations of cosmology* (Cambridge University Press, Oxford, 2005) p. 319.

Supplementary Material for Parametric-Resonance Production of QCD Axions

Pirzada, Yu Gao, Qiaoli Yang

This Supplementary Material provides additional calculations and derivations supporting the results in the main text.

Fourier-space equation of motion

To connect Eq. (2) to the mode-by-mode evolution used earlier, we Fourier transform the field and perturbations using the convention

$$\phi(\vec{x}, t) = \int \frac{d^3 k}{(2\pi)^3} e^{i\vec{k}\cdot\vec{x}} \phi_{\vec{k}}(t). \quad (\text{A1})$$

The same applies to $\Psi(\vec{x}, t)$ and $\delta T(\vec{x}, t)$. Substituting into Eq. (2), the homogeneous part becomes diagonal in \vec{k} :

$$\ddot{\phi}_{\vec{k}} + 3H\dot{\phi}_{\vec{k}} + \left(\frac{k^2}{a^2} + m^2(T(t)) \right) \phi_{\vec{k}} + f_{\vec{k}}(t) = 0, \quad (\text{A2})$$

where $k \equiv |\vec{k}|$ and $f_{\vec{k}}$ is the Fourier transform of $f(\vec{x}, t, \phi)$. Since f contains products of perturbations with ϕ and its derivatives, its Fourier transform generally involves a convolution over intermediate momenta [39]:

$$f_{\vec{k}}(t) = \int \frac{d^3 q}{(2\pi)^3} \mathcal{K}(\vec{k}, \vec{q}; t), \quad (\text{A3})$$

The kernel \mathcal{K} is obtained by transforming each term in f . Explicitly,

$$\begin{aligned} f_{\vec{k}}(t) = & -2 \int \frac{d^3 q}{(2\pi)^3} \Psi_{\vec{k}-\vec{q}}(t) \ddot{\phi}_{\vec{q}}(t) - \int \frac{d^3 q}{(2\pi)^3} \left(\dot{\Psi}_{\vec{k}-\vec{q}} - 3\dot{\Phi}_{\vec{k}-\vec{q}} + 6H\Psi_{\vec{k}-\vec{q}} \right) \dot{\phi}_{\vec{q}} + \frac{2}{a^2} \int \frac{d^3 q}{(2\pi)^3} \Phi_{\vec{k}-\vec{q}}(t) (-q^2) \phi_{\vec{q}}(t) - \frac{1}{a^2} \\ & \int \frac{d^3 q}{(2\pi)^3} i(\vec{k} - \vec{q}) \cdot i\vec{q} (\Phi_{\vec{k}-\vec{q}} + \Psi_{\vec{k}-\vec{q}}) \phi_{\vec{q}}(t) + \frac{dm^2}{dT} \int \frac{d^3 q}{(2\pi)^3} \delta T_{\vec{k}-\vec{q}}(t) \phi_{\vec{q}}(t). \end{aligned} \quad (\text{A4})$$

Equations (A2) and (A4) fully Fourier-transform Eq. (2). In general, perturbations mediate mode coupling through convolutions.

In the regime relevant to linear response calculations, namely with small metric potentials and a prescribed stochastic background characterized by $\Phi_p(\vec{k})$, it is standard practice to isolate the evolution of each Fourier mode $\phi_{\vec{k}}$ by treating gravitational potentials as external fields and neglecting mode-mixing beyond leading order in Φ_p . Under this approximation, convolution integrals reduce to multiplicative modulations for individual \vec{k} -modes, and Eq. (A2) simplifies to a closed equation with decoupled modes, with time-dependent coefficients sourced by $\Phi(\vec{k}, t)$ and $\delta T(\vec{k}, t)$. During radiation domination and for modes well inside the horizon ($k\eta \gg 1$), the metric potential $\Phi(\vec{k}, t)$ adopts its standard form [29, 40].

Full equation of a Mathieu form

Writing Eq. (5) schematically:

$$\left[1 - \alpha(t) \cos \Theta \right] \ddot{\phi}_k + \left[\gamma_0(t) + \gamma_1(t) \sin \Theta + \gamma_2(t) \cos \Theta \right] \dot{\phi}_k + \left[\omega_k^2(t) + \delta\omega^2(t) \cos \Theta \right] \phi_k = 0, \quad (\text{A5})$$

with coefficients:

$$\begin{aligned} \alpha(t) &= \frac{9\Phi_p}{2k^2 t t_1}, \quad \gamma_0(t) = \frac{3}{2t}, \\ \omega_k^2(t) &= \frac{k^2}{a^2(t)} + m^2(t) = k^2 \frac{t_1}{t} + m^2(t), \\ \text{and } \delta\omega^2(t) &= \frac{9\Phi_p}{2t^2} - \frac{3\Phi_p}{2} \frac{dm^2(t)}{d \ln T}. \end{aligned} \quad (\text{A6})$$

Near the resonance time $t \approx t_R(k)$, we assume a narrow window Δt where:

$$\Delta t \ll t_R, \quad \left| \frac{\omega_k}{\omega_k} \right| \Delta t \ll 1, \quad \left| \frac{\delta\omega^2}{\delta\omega^2} \right| \Delta t \ll 1, \quad (\text{A7})$$

This allows treating $\omega_k^2(t)$ and $\delta\omega^2(t)$ as approximately constant while trigonometric terms oscillate rapidly. Neglecting Hubble friction and small modulations, Eq. (A5) reduces to:

$$\ddot{\phi}_k + \left[\omega_k^2(t_R) + \delta\omega^2(t_R) \cos \Theta_k(t) \right] \phi_k \simeq 0. \quad (\text{A8})$$

Define a rescaled time variable:

$$z \equiv \frac{\Theta_k(t)}{2} = \frac{k}{\sqrt{3}} \sqrt{t_1 t} = \frac{k}{2\sqrt{3}} \eta(t), \quad \Rightarrow \quad \cos \Theta_k(t) = \cos(2z). \quad (\text{A9})$$

Within the resonance window, \dot{z} is approximately constant. Using $\dot{\phi} = \dot{z} \phi'$ and $\ddot{\phi} \simeq \dot{z}^2 \phi''$ (primes denote d/dz), we obtain:

$$\phi_k'' + \left[\frac{\omega_k^2(t_R)}{\dot{z}^2} + \frac{\delta\omega^2(t_R)}{\dot{z}^2} \cos(2z) \right] \phi_k \simeq 0. \quad (\text{A10})$$

Comparing to the canonical Mathieu equation:

$$\phi_k'' + (A_k - 2q \cos(2z)) \phi_k = 0, \quad (\text{A11})$$

we identify parameters:

$$A_k(t_R) = \frac{\omega_k^2(t_R)}{\dot{z}^2}, \quad -2q(t_R) = \frac{\delta\omega^2(t_R)}{\dot{z}^2}. \quad (\text{A12})$$

Using $\omega_k^2 = k^2/a^2 + m^2$ and $\dot{z}^2 = k^2/(12a^2)$, we recover the standard Mathieu parameters A_k and q . For small $|q|$, instability tongues emerge near $A_k \simeq \ell^2$, with the resonance centers at $A_k(t_R) = \ell^2$. Under a standard rescaling (where the Mathieu parameter A_k is normalized by 4), the dominant instability band corresponds to $\ell = 2$, centered at $A_k \simeq 4$. This reflects a time-local commensurability between the oscillator frequency and the driving term:

$$A_k(t_R) \simeq 4 \iff \frac{m(t_R)a(t_R)}{k} \simeq \frac{1}{\sqrt{3}} \iff k_{\text{phys}}(t_R) \simeq \sqrt{3}m(t_R). \quad (\text{A13})$$

For a power-law mass model $m(T) \propto T^{-n}$, this condition reduces to the resonance criterion: *Case 1: Resonance during growth* ($t_R < t_2$). Substitute $m(t_R) = m(t_R/t_2)^n$ into Eq. (A13):

$$k^2 \frac{t_1}{t_R} = 3m^2 \left(\frac{t_R}{t_2} \right)^{2n} \Rightarrow t_R^{2n+1} = \frac{k^2 t_1 t_2^{2n}}{3m^2}. \quad (\text{A14})$$

Define

$$k_2 \equiv m \sqrt{\frac{3t_2}{t_1}}, \quad (\text{A15})$$

which gives

$$t_R = t_2 \left(\frac{k}{k_2} \right)^{\frac{2}{2n+1}} \quad (k < k_2). \quad (\text{A16})$$

Case 2: Resonance after saturation ($t_R > t_2$). Set $m(t_R) = m$ in Eq. (A13):

$$k^2 \frac{t_1}{t_R} = 3m^2 \Rightarrow t_R = \frac{k^2 t_1}{3m^2} = t_2 \left(\frac{k}{k_2} \right)^2 \quad (k > k_2), \quad (\text{A17})$$

this matches the main text's derived condition, validating consistency across both regimes.